

Analysis of the Effect of Al on the Static Softening Kinetics of C-Mn Steels Using a Physically Based Model

ZALOA ARETXABALETA, BEATRIZ PEREDA, and BEATRIZ LÓPEZ

The effect of Al addition on the static softening behavior of C-Mn steels was investigated. Double-hit torsion tests were performed at different deformation temperatures ranging from 1198 K to 1338 K (925 °C to 1065 °C) with pass strains of $\varepsilon = 0.2$ and 0.35. It was found that solute Al produced a significant delay on the static softening kinetics. Additionally, at the lowest temperatures [1198 K to 1238 K (925 °C to 965 °C)] and highest Al level (2 wt pct), austenite to ferrite phase transformation was found to be concurrent with softening, leading this to higher softening retardation. The softening kinetics of the steels investigated were analyzed using a physically based model which couples recovery and recrystallization mechanisms. The main parameters of the model were identified for the present alloys. An expression for the grain boundary mobility of the base C-Mn steel was derived and the retarding effect of Al in solid solution on the static recrystallization kinetics was introduced in the model. Reasonable agreement was obtained between model and experimental results for a variety of deformation conditions.

DOI: 10.1007/s11661-013-2014-2

© The Minerals, Metals & Materials Society and ASM International 2013

I. INTRODUCTION

IN the past decades, extensive research on the effect of processing parameters on the microstructures and mechanical properties of hot rolled steels has been carried out and several models based on semi-empirical equations have been developed.^[1–3] However, recently there has been a trend to develop more physically based models. The latter present several advantages compared to empirical equations: they are not limited to the conditions they were developed for, and in addition, they can provide valuable insight into the processes that occur during hot rolling. Nevertheless, there are also some limitations related to physical models, such as uncertainty in the values of some of the parameters involved in the equations employed or how alloying elements can affect softening processes.

Several authors have investigated the application of physical models to the microstructural evolution of steels during and after hot deformation. During deformation, the internal energy of the austenite is increased through the storage of dislocations. After deformation, the energy stored in the material can decrease due to two different mechanisms: recovery, defined as the continuous rearrangement and annihilation of dislocations, or through recrystallization, which consists of the nucleation and growth of new grains free of dislocations into the deformed matrix. Since the driving force for both mechanisms is the stored energy of deformation, the

progression of recovery may reduce the driving force available for recrystallization, leading to retardation in recrystallization progression.^[4] As a result, in order to model microstructural evolution of austenite, physical models must consider the coupled effect of these two processes.

In addition to the effect of deformation and annealing parameters, the effect of microalloying elements on recovery and recrystallization must be taken into account. The effect of conventional microalloying elements, such as Nb, Ti, V or Mo in solid solution on the static softening kinetics of the austenite has been widely studied and it has been shown that they lead to a significant retardation on static softening processes.^[5,6] Retardation on recrystallization kinetics has usually been attributed to a reduction in grain boundary mobility due to the solute drag effect. Although less studied, works which indicate that elements in solid solution can also retard recovery kinetics are as well found in the literature.^[7] However, most of these studies have been carried out from an empirical point of view, and as a result, it is difficult to extrapolate the results to different conditions.

Moreover, these studies all concentrated on conventional microalloying additions. However, in recent years, new steel alloying concepts have been developed. An example of this new steel design trend is TRIP-assisted steels, which are currently considered as good candidates for maintaining steel as a leading material in the automotive industry due to the good strength and ductility balance and excellent formability that they exhibit. These grades present a multiphase room microstructure consisting of ferrite and bainite and a smaller volume fraction of high-C retained austenite (~10 pct), which during deformation transforms into martensite resulting in high uniform elongation levels. Usually, in

ZALOA ARETXABALETA, Ph.D. Student, BEATRIZ PEREDA, Researcher, and BEATRIZ LÓPEZ, Professor, are with the CEIT and TECNUN, University of Navarra, Pº de Manuel Lardizabal, 15, 20018 Donostia-San Sebastián, Basque Country, Spain. Contact e-mail: blopez@ceit.es

Manuscript submitted March 15, 2013.

Article published online October 1, 2013

order to obtain the desired microstructure, a two-step thermal cycle and alloying with high Si levels (~1.5 pct) are employed. However, high Si levels also impair the steel surface quality and galvanizability, and as a consequence, partial or complete substitution of Si by Al has been proposed.^[8,9]

Studies of the microstructures and mechanical properties of CMnAl and CMnAlSi TRIP-aided steels have been carried out and have been shown to be comparable to those obtained in conventional Si-alloyed steels.^[9–11] However, much less attention has been paid to the hot working mechanism characterization of high Al steels. Some data which indicate that Al has an influence on the stress levels and the dynamic softening kinetics have been reported.^[12] More recently, Suikkanen *et al.*^[13] have found that Al has a more significant retardation effect on static recrystallization than Si. The aim of this work is to investigate the effect of Al addition on the static softening behavior of these steels. In order to do so, torsion tests were carried out with a base C-Mn and two steels alloyed with Al levels similar to those employed in TRIP-assisted steels. The static softening kinetics were determined experimentally at different temperatures and deformation conditions, and several specimens were quenched in order to determine the different microstructural events occurring after deformation. The experimental data obtained were then used to fit the parameters of a physically based model, which takes into account the interaction between recrystallization and recovery.

II. EXPERIMENTAL

Three steels with compositions representative of TRIP-assisted grade steels were studied. The three casts were produced in the laboratory with the chemical compositions listed in Table I. Two levels of Al addition, 1 pct (C2Mn2Al1) and 2 pct (C2Mn2Al2), and a reference steel (C2Mn2) were considered. The ingots were rolled in the laboratory to 25-mm-thick plates from which torsion samples were machined.

Double and single hit torsion tests were carried out to characterize the softening behavior of the steels. The gage section of the torsion specimens was 16.5 mm in length and 7.5 mm in diameter. The specimens were soaked at 1523 K (1250 °C) during 15 min and cooled down to the selected deformation temperature.

In the case of the double deformation tests, once the temperature was stabilized the specimen was prestrained at a constant strain rate of 1 s^{-1} , unloaded and held for increasing times to enable softening processes to occur. After the interruption, the specimens were reloaded to

$\varepsilon = 0.1$ at the same temperature and strain rate conditions. From the flow curves, the fractional softening was determined using the 2 pct offset method.^[14] According to this method, the softening corresponding to each interpass time can be calculated as follows:

$$X_{\text{SOFT}} = \frac{\sigma_m - \sigma_r}{\sigma_m - \sigma_0}, \quad [1]$$

where σ_m is the maximum stress of the first flow curve, and σ_0 and σ_r are the offset yield stresses determined in the first and second curves, respectively, using a plastic strain of 2 pct. The values of σ_m , σ_0 , and σ_r represent the flow stresses for the work hardened, completely softened, and partially softened material, respectively. In the tests, pass strains of $\varepsilon = 0.2$ and 0.35 and deformation temperatures ranging from 1338 K to 1198 K (1065 °C to 925 °C) were employed.

The Thermo-Calc software (TCFE 6 database)^[15] was used in order to investigate the effect of Al addition on the equilibrium phases obtained at different temperatures. Some specimens were quenched directly after the soaking treatment to characterize the microstructure of the steels before deformation. In addition, several specimens were quenched after single-pass deformation tests and prepared for metallographic analysis. The aim was to investigate the microstructural evolution of the steels after deformation at different temperatures and interpass times and to characterize the statically recrystallized microstructure after deformation at different conditions.

Metallographic analysis of the quenched samples was carried out on a section corresponding to 0.9 of the outer radius of the torsion specimen, R , also known as the sub-surface section.^[16] The specimens were etched either with a picric-based etchant in order to reveal the prior austenite grain boundaries or with a solution of 2 pct HNO₃ in ethanol (2 pct Nital) in order to identify the presence of ferrite in the microstructure. The austenite grain sizes were measured using Leica Qwin v.5.3.1 Image Analysis software in terms of the mean equivalent diameter parameter.

III. RESULTS

A. Initial Microstructure

Figure 1 shows the equilibrium austenite and ferrite mole phase fractions calculated by the Thermo-Calc software at different temperatures for the three steel compositions studied in this work. From the figure it can be observed that Al addition leads to a significant increase in the ferrite phase equilibrium stability and in the A_{e3} temperature, which is in good agreement with the trends reported in other works.^[8,9] According to the calculations, 1 pct Al addition (C2Mn2Al1 steel) raises the A_{e3} temperature from 1053 K to 1173 K (780 °C to 900 °C), while 2 pct Al addition results in a further increase of up to 1303 K (1030 °C). It must be noted that the deformation temperature employed during some of the torsion tests for the C2Mn2Al2 steel is below the predicted A_{e3} temperature.

Table I. Composition of the Steels Studied (Wt pct)

Steel	C	Si	Mn	P	S	Nb	Al	N
C2Mn2	0.195	0.011	1.98	0.01	0.001	0.001	0.028	0.005
C2Mn2Al1	0.210	0.010	2.04	0.02	0.001	0.001	1.060	0.005
C2Mn2Al2	0.200	0.020	1.99	0.02	0.001	0.001	2.010	0.005

It must be mentioned that Thermo-Calc also predicts the presence of AlN phase in the range of temperatures investigated. This could be of interest regarding the softening behavior of the steels, firstly because AlN precipitation could lead to a decrease in the amount of Al in solid solution, and secondly because strain-induced precipitation of second phase particles is known to influence the softening behavior of microalloyed steels. However it must be taken into account that the maximum AlN mole fraction which can be formed is limited by the N content and as a result the Al amount which can be tied up in the form of AlN is the same and very low (<0.01 wt pct) for the three steels. The calculations also indicate that for the two highest Al contents (1 and 2 pct), nearly all the AlN present in the microstructure remains undissolved during the reheating treatment. The analysis of the C2Mn2Al1 and C2Mn2Al2 steel specimens quenched after the soaking treatment by means of Scanning Electron Microscopy (SEM) confirmed the presence of very coarse (>1 μm) Al and N bearing particles, which are not expected to affect the softening behavior of the steels investigated. Therefore, for these steels an effect of Al in solid solution can be expected after deformation only.

In Figure 2, several micrographs corresponding to the microstructures obtained for the three steels after the soaking treatment at 1523 K (1250 °C) etched with a

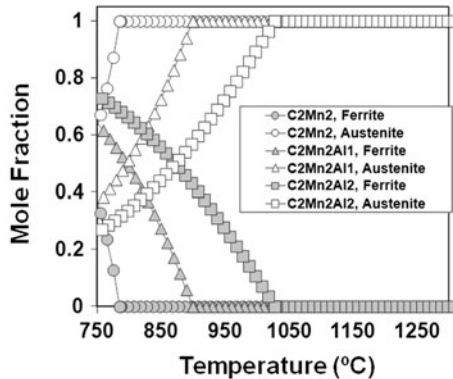


Fig. 1—Equilibrium austenite and ferrite mole fractions predicted by the Thermo-Calc software (TCFE 6 database) for the steel compositions studied in this work.

picric-based solution are shown. In the case of the C2Mn2 and C2Mn2Al1 steels, fully austenitic microstructures, with austenite average sizes of $69 \pm 4 \mu\text{m}$ and $100 \pm 3 \mu\text{m}$, respectively, were obtained. In the case of the C2Mn2Al2 steel, the micrograph denotes that there are two different constituents, each with very different grain sizes, present in the microstructure. After etching with a 2 pct Nital solution (2 pct HNO_3 in ethanol), the coarse grains were identified as martensite, a product of the quenched austenite, and the smallest grains were identified as ferrite. The results indicate that after soaking at 1523 K (1250 °C), the C2Mn2Al2 steel presents a duplex microstructure with an austenite average grain size of $65 \pm 2 \mu\text{m}$ and a small amount of ferrite. Although this finding differs from the thermodynamic predictions shown above (single austenite phase is predicted to be present at 1523 K (1250 °C) in Figure 1), it must be mentioned that the ferrite percentage found in the quenched specimens was very small, ~2 pct, and could be due to the fact that the time spent in the reheating treatment, 15 min, was not long enough to achieve thermodynamic equilibrium. On the other hand, it was also observed that the ferrite grains appeared in bands and aligned with the rolling direction in the plates, which suggests that Al microsegregation in the original slab could also be in part cause of the presence of the ferrite in these areas. The amount of ferrite found in the microstructure, ~2 pct, was considered too small to have any effect on the softening kinetics of the deformed C2Mn2Al2 specimens.

B. Softening Kinetics

In Figure 3, the fractional softening results obtained for the three steels at different deformation temperatures and pass strains are shown. In all the cases, the experimental data can be well fitted to an Avrami type equation:

$$X_{\text{SOFT}} = 1 - \exp\left(-0.693\left(\frac{t}{t_{0.5}}\right)^n\right), \quad [2]$$

where X_{SOFT} is the fractional softening corresponding to a time t , $t_{0.5}$ is the time to reach 50 pct softening, and n is the Avrami exponent.

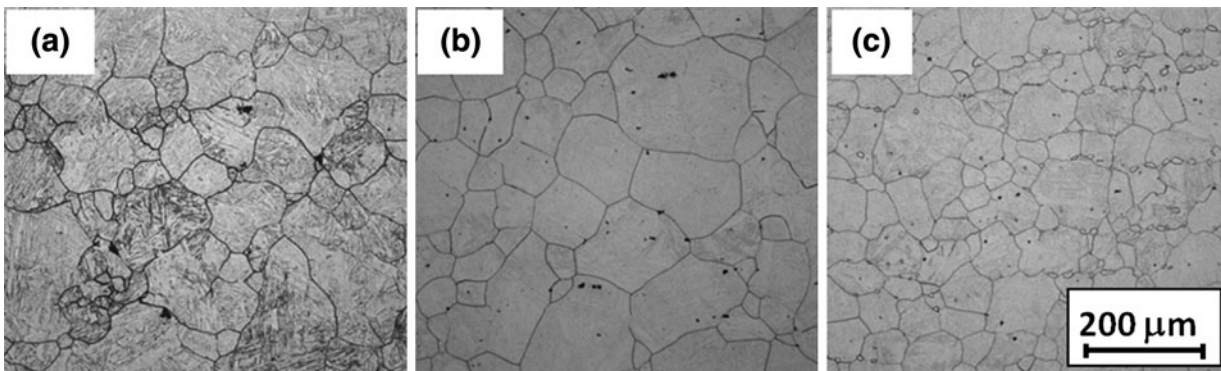


Fig. 2—Microstructures obtained after soaking for the (a) C2Mn2, (b) C2Mn2Al1, and (c) C2Mn2Al2 steels.

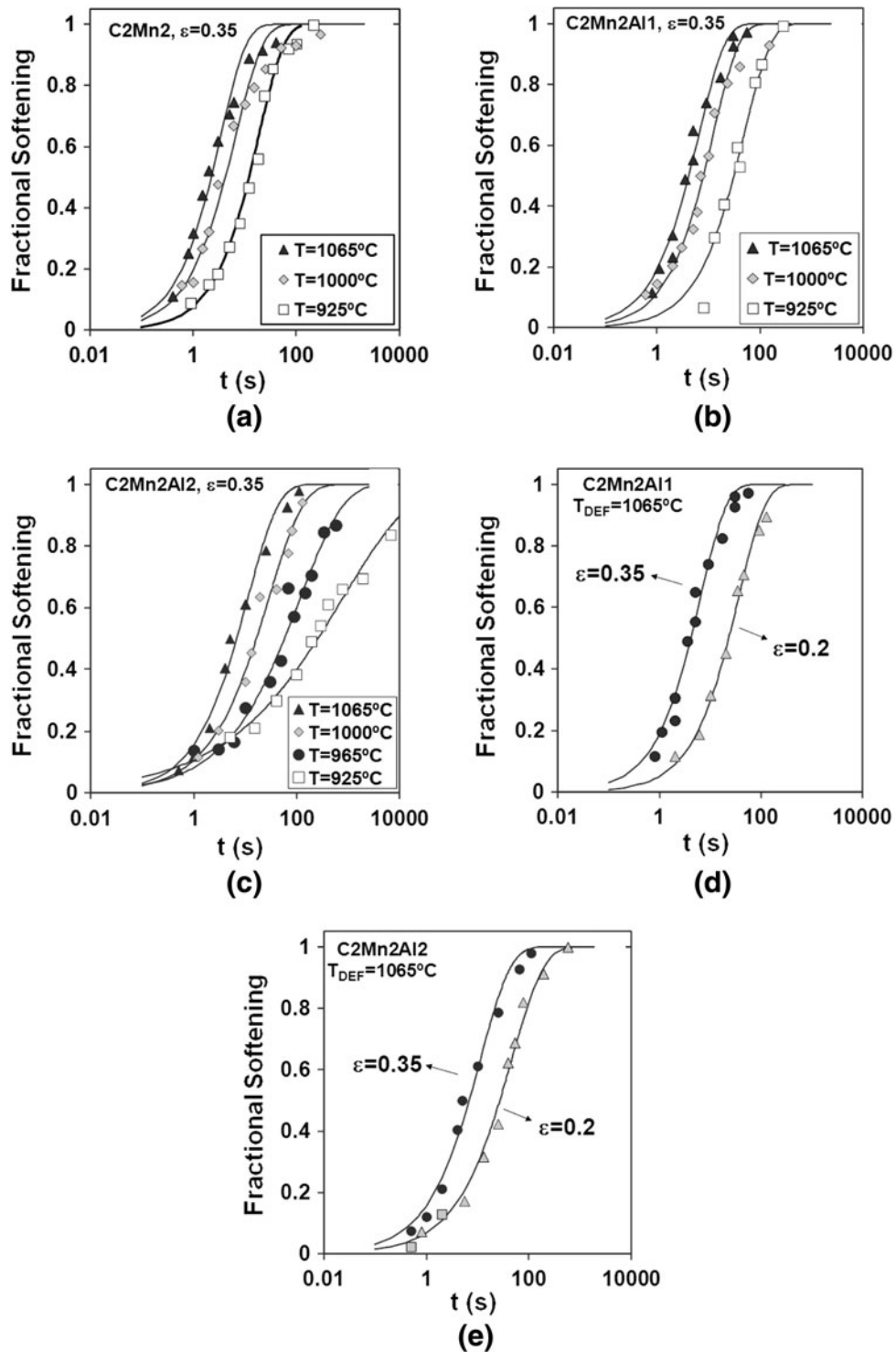


Fig. 3—Softening curves obtained for steels (a) C2Mn2, (b) C2Mn2Al1, and (c) C2Mn2Al2 at different deformation temperatures and for (d) C2Mn2Al1 and (e) C2Mn2Al2 at different pass strains.

As it is usually reported in the literature, increasing the pass strain or the deformation temperature leads to faster softening kinetics in every case. From the figures, it can also be noted that for the C2Mn2 and C2Mn2Al1 steels, the n Avrami exponent is approximately constant, taking a value of $n \sim 0.8$, which is

not affected by the change in pass strain or deformation temperature. In the case of the C2Mn2Al2 steel, however, decreasing deformation temperature results in a significant reduction of the n Avrami exponent, from $n = 0.73$ at 1338 K (1065 °C) to $n = 0.32$ at 1198 K (925 °C).

In order to evaluate the effect of Al addition on the softening kinetics, a normalized time, which excludes the effect of deformation conditions and initial microstructure, $\tau_{0.5}$, was calculated based on the equation proposed by Fernandez *et al.*^[2] for the 50 pct softening time as follows:

$$\tau_{0.5} = \frac{t_{0.5}}{D_0 \cdot \varepsilon^{-5.6} D_0^{-0.15} \cdot \dot{\varepsilon}^{-0.53}}, \quad [3]$$

where D_0 is the initial austenite grain size (μm), ε and $\dot{\varepsilon}$ the applied strain and strain rate (s^{-1}), respectively. The values obtained for the three steels at different deformation temperatures are plotted in Figure 4. The figure shows that Al addition produces retardation in the normalized 50 pct softening $\tau_{0.5}$ time. This effect is more important for the highest Al content (2 pct), especially at the lowest deformation temperatures of 1238 K and 1198 K (965 °C and 925 °C).

In order to investigate the mechanisms leading to softening retardation, several specimens were quenched after deformation and their microstructure analyzed. Figure 5 shows the microstructures obtained for the C2Mn2Al1 steel after deformation at 1338 K (1065 °C) ($\varepsilon = 0.35$) and at different holding times (etching with the picric acid agent). At early softening stages ($t = 2$ seconds, Figure 5(a)), small nuclei start to

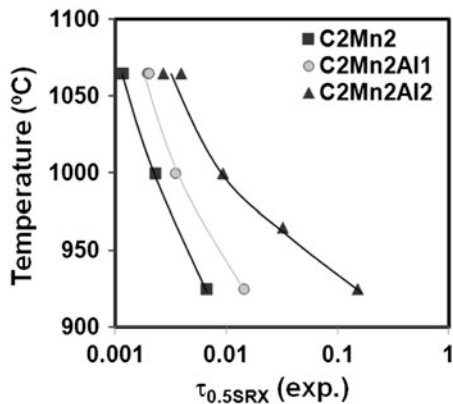


Fig. 4—Normalized 50 pct fractional softening time for the steels studied in this work at different temperatures.

develop in the microstructure, which indicates static recrystallization onset. As recrystallization progresses (Figure 5(b)), these grains grow until a completely recrystallized microstructure is obtained (Figure 5(c)), with an average grain size that is slightly refined compared to the initial austenite grain size.

In the figure caption, both the recrystallized fraction determined by metallographic means and the fractional softening levels obtained from the double-hit torsion tests are also indicated. It must be mentioned that the similar size of the initial and the recrystallized grains makes it quite difficult to detect the recrystallized grains, and therefore the metallographic measurements must be considered as an approximation. In order to carry out these measurements, parameters such as the elongation in the deformation direction and the grain boundary curvature were taken into account. It is interesting to note that at initial softening stages ($t = 2$ seconds), there is a significant difference between the recrystallized fraction, 2 pct, and the fractional softening level, 31 pct. As time increases ($t = 5$ seconds), the difference is reduced, 35 pct recrystallized for 55 pct softened fraction, and both values finally converge when softening reaches completion ($t = 30$ seconds). The difference between softening and recrystallization levels at the first softening stages has also been observed by other authors,^[17,18] and it is generally attributed to the effect of recovery.

Specimens corresponding to the C2Mn2Al2 steel quenched after deformation were also analyzed. Micrographs corresponding to some of these specimens deformed at 1198 K (925 °C) ($\varepsilon = 0.35$) and quenched after different holding times, etched with 2 pct Nital, are shown in Figure 6. In the pictures, dark areas correspond to martensite phase coming from quenched austenite. Figure 6(a), which shows the microstructure obtained just after deformation, indicates that it contains a very low ferrite fraction similar to that found in the initial microstructure. However, by increasing the holding time after deformation to 270 seconds, which corresponds to approximately 50 pct fractional softening, a substantial increase in the ferrite percentage is detected, from 1 pct to 33 pct. This indicates that $\gamma \rightarrow \alpha$ phase transformation is taking place concurrently with mechanical softening after deformation. Moreover,

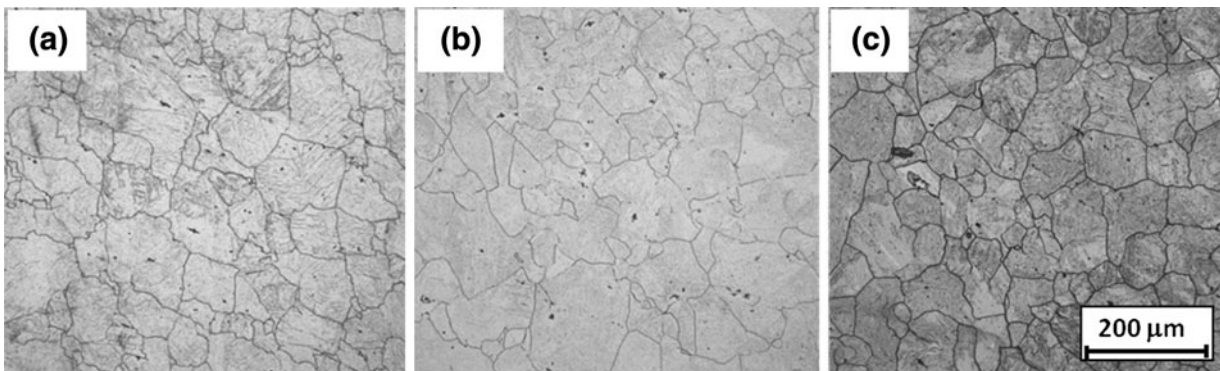


Fig. 5—Microstructures of specimens corresponding to steel C2Mn2Al1 after straining at 1338 K (1065 °C) ($\varepsilon = 0.35$) and quenched after different holding times (a) $t = 2$ s, $X_{\text{REX}} \sim 2 \pm 1$ pct, FS = 31 pct, (b) $t = 5$ s, $X_{\text{REX}} \sim 35 \pm 2$ pct, FS = 55 pct and (c) $t = 30$ s, $X_{\text{REX}} \sim 100$ pct.

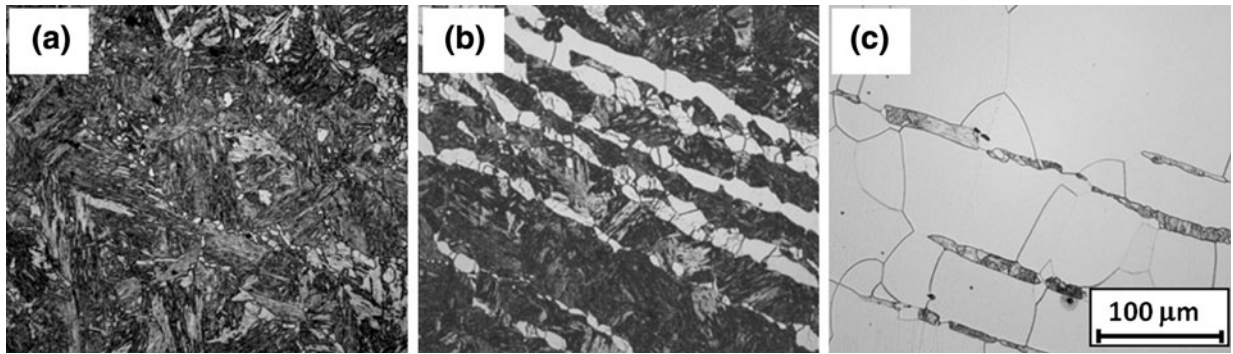


Fig. 6—Microstructure of specimens corresponding to the C2Mn2Al2 steel after deformation at 1198 K (925 °C) and quenched at different holding times: (a) $t = 0$ s, (b) $t = 270$ s, FS = 50 pct, $f_x = 0.33$, and (c) $t = 10200$ s, FS = 90 pct, $f_x \approx 1$.

Table II. Recrystallized Grain Sizes Measured After Deformation at Different Conditions

Steel	T [K (°C)]	D_0 (μm)	ε	D_{REX} (μm)
C2Mn2Al1	1338 (1065)	100 ± 3	0.2	95 ± 5
	1338 (1065)		0.35	62 ± 3
	1198 (925)		0.35	53 ± 2
C2Mn2Al2	1338 (1065)	65 ± 1	0.2	68 ± 2
	1338 (1065)		0.35	60 ± 2
	1273 (1000)		0.35	52 ± 2
C2Mn2	1338 (1065)	69 ± 4	0.2	67 ± 2
	1338 (1065)		0.35	56 ± 2
	1198 (925)		0.35	62 ± 3

Figure 6(c) shows that the microstructure corresponding to 90 pct fractional softening ($t = 10200$ seconds) is mainly constituted by very coarse ferrite grains, indicating that as the mechanical softening progresses, phase transformation has nearly been completed and ferrite grain growth has also occurred.

In order to investigate whether the microstructure evolution for the C2Mn2Al2 steel followed a similar trend at other temperatures specimens quenched after deformation at higher temperatures were also analyzed. In the case of the specimen quenched after deformation at 1238 K (965 °C) for a time corresponding to 50 pct softening ($t = 60$ seconds), a significant ferrite fraction was also measured ($f_x = 0.18$), meaning that at 1238 K (965 °C) austenite to ferrite phase transformation is also taking place concurrently with mechanical softening. At 1273 K (1000 °C) or above, conversely, no evidence of phase transformation was observed, which is in good agreement with the thermodynamic calculations (see Figure 1).

The recrystallized grain sizes obtained after complete softening were also measured in those cases where fully austenitic microstructures were obtained. The resulting values are summarized in Table II. From the data, no significant effect of temperature on the recrystallized grain size is observed. However, decreasing the applied strain leads in all cases to an increase in the austenite grain size. This behavior is in good agreement with that reported by other authors who only have found an effect of the initial grain size and strain, but none for temperature.^[1,19,20]

The above results indicate that for the C2Mn2Al2 steel at temperatures above 1238 K (965 °C), the

microstructural events operating in the austenite are recrystallization and recovery, with both mechanisms contributing to austenite softening after deformation, whereas at 1238 K and 1198 K (965 °C and 925 °C) austenite to ferrite phase transformation also occurs simultaneously with mechanical softening. As previously shown in Figure 4, this increase in the ferrite fraction is accompanied by significant retardation in the softening kinetics and a high decrease in the n Avrami exponent. A similar trend was observed in a previous work, in which a high increase in the T_{nr} was observed in multipass torsion tests carried out with C2Mn2Al2 steel also related to the occurrence of austenite to ferrite phase transformation.^[21] Bearing in mind that for both, phase transformation and recrystallization processes, the main nucleation sites are the austenite grain boundaries, a possible explanation of the observed softening retardation is that when phase transformation initiates, recrystallization is nearly prevented. If the sites available for nucleation of new recrystallized grains are first occupied by ferrite grains, further softening of the austenite by recrystallization would be practically avoided, and only recovery could take place in this phase. As a result, all the softening occurring after deformation might be mainly attributed to phase transformation.

The results indicate that the softening data determined for the C2Mn2Al2 steels at temperatures below 1273 K (1000 °C) cannot be considered representative of static recrystallization occurrence. However, the results obtained at higher temperatures for both Al bearing steels show that this alloying element produces noticeable retardation in the softening kinetics of the austenite. In order to evaluate this effect, the applicability of a physically based model, which takes into account the simultaneous effect of recrystallization and recovery, was investigated.^[4]

IV. MODELING APPROACH

Recrystallization evolution is modeled based on the JMAK approach. Assuming a random distribution of nuclei and site-saturation conditions, the evolution of the recrystallized fraction with time can be expressed as^[22]:

$$X_{\text{REX}} = 1 - \exp \left[-N_{\text{REX}} \left(\int_0^t M(t) F_{\text{REX}} dt \right)^3 \right], \quad [4]$$

where N_{REX} is the initial number of recrystallization nuclei, F_{REX} the driving force for recrystallization, and $M(t)$ the grain boundary mobility. The F_{REX} can be related to the instantaneous dislocation density, $\rho(t)$, through a relationship of the type:

$$F_{\text{REX}} = \frac{1}{2} \rho(t) \mu b^2 \quad [5]$$

In this equation μ is the temperature (T) dependent shear modulus of the matrix ($\mu = 81 \times 10^9 \cdot [0.91 - (T(K) - 300)/1810] \text{ Pa}^{[24]}$) and b is the Burgers vector. $\rho(t)$ is related to the flow stress of the austenite through a forest type hardening relation^[23]:

$$\sigma(t) = \sigma_y + M \alpha_T \mu b \sqrt{\rho(t)}, \quad [6]$$

where σ_y is the yield stress, M the Taylor factor ($M = 3.1$ for FCC metals), and α_T a constant of the order of 0.15.^[4]

The recovery kinetics is modeled using the approach of Verdier *et al.*^[25] In their model, the rate of change of internal stress due to the dislocations is expressed as:

$$\frac{d(\sigma(t) - \sigma_y)}{dt} = - \frac{64(\sigma(t) - \sigma_y)^2 v_d}{9M^3 \alpha_T^2 E} \exp\left(-\frac{U_a}{kT}\right) \times \sinh\left(\frac{(\sigma(t) - \sigma_y) V_a}{kT}\right), \quad [7]$$

where E is Young's modulus ($E = 2\mu(1 + 0.33) \text{ Pa}^{[24]}$), v_d is the Debye frequency, and U_a and V_a are the activation energy and activation volume for the recovery process. Following Reference 26, the activation volume can be expressed as:

$$V_a = b^2 l_a, \quad [8]$$

where l_a is an activation length which varies depending on the recovery controlling mechanism. If either climb of edge dislocations or glide of jogged screw dislocations are the recovery rate controlling mechanisms, the activation length can be approximately described by Reference 27:

$$l_a = \frac{K_1}{\sqrt{\rho}}, \quad [9]$$

where K_1 is a constant. Combining equations [6], [8], and [9] yields a value for the activation length due to dislocations of:

$$l_a = \frac{K_1 M \alpha_T \mu b}{\sigma - \sigma_y} \quad [10]$$

The initial dislocation density and the recrystallization driving force can be calculated from the experimental flow curves through Eqs. [6] and [5], respectively. Recrystallization progression after deformation is

evaluated by the numerical integration of Eq. [4]. At each time interval, the dislocation density diminution due to recovery is calculated using Eqs. [6] and [7]. The instantaneous dislocation density is then used as input for Eq. [5], thus taking the effect of recovery on the driving force for recrystallization into account.

Several works have discussed the application of physical models in order to predict the softening kinetics of austenite. However, there are still uncertainties concerning the values of some of the parameters involved, and some of them can vary depending on steel composition. In the case of recrystallization, the number of recrystallization nuclei, N_{REX} , the driving force for recrystallization, F_{REX} , and grain boundary mobility $M(t)$ can be affected by steel composition. In the case of recovery, both the activation energy and volume, U_a and V_a , have also been reported to be dependent on both steel composition and deformation conditions.^[27]

V. DISCUSSION

A. Calculation of Model Parameters

1. Base C-Mn steel

First, modeling of the softening evolution in the base C-Mn steel was undertaken. To allow a comparison with the experimental softening data, a simulated fractional softening value is calculated (see Eq. [1]). The yield stress of the initial softened material, σ_0 , and of the deformed material, σ_m , are obtained from the experimental flow curves for each test condition. The value of the partly softened material, σ_r , varies with interpass time and can be calculated using a mixture rule that combines the recrystallized fraction at each time, X_{REX} (obtained from the recrystallization model (Eq. [4]) coupled to the recovery model), with the stress present in the unrecrystallized material at each step, $\sigma(t)$, which is calculated from the recovery model (Eq. [7]):

$$\sigma_r = X_{\text{REX}} \sigma_{\text{REX}} + (1 - X_{\text{REX}}) \sigma(t) \quad [11]$$

In the above equation, σ_{REX} is the value of the yield stress of the fully recrystallized matrix. In the absence of precipitation, only the effect of the grain size difference between the initial undeformed and recrystallized material on the stress level should be taken into account in determining σ_{REX} . In order to do so, the following dependence proposed by Yoshie *et al.*^[28] has been considered:

$$\sigma_{\text{REX}} = \sigma_0 \left(\frac{D_{\text{REX}}}{D_0} \right)^{-0.07}, \quad [12]$$

where D_0 is the initial grain size and D_{REX} the grain size of the recrystallized microstructure.

In this work, the number of nuclei, N_{REX} , was estimated through the experimentally measured recrystallized grain size, D_{REX} (Table II), as:

$$N_{\text{REX}} = \left[\frac{4}{3} \pi \left(\frac{D_{\text{REX}}}{2} \right)^3 \right]^{-1} \quad [13]$$

The recrystallization driving force, F_{REX} , was calculated from the experimental flow stress curves by applying equations [5] and [6].

The activation energy for the recovery process, U_a , is expected to lie between 0.6 and 1 Q_{diff} , where Q_{diff} is the activation energy for self-diffusion or solute-diffusion, depending on the recovery rate controlling process.^[27] The self-diffusion activation energy of the austenite ~286 kJ/mol is higher than the activation energy for the diffusion of the alloying elements commonly considered to retard softening processes in austenite (~260 to 270 kJ/mol for Nb or Mn), and therefore values close to 286 kJ/mol have been employed in different works.^[4,29] In terms of the determination of the activation volume for recovery, V_a , several authors have used stress relaxation tests.^[30,31] However, there is a considerable spread within the determined values, ranging from 15 b^3 to 45 b^3 ^[32] or 230 to 690 b^3 ,^[31] with b the Burgers vector. Bearing in mind that steel composition and deformation conditions can have an influence on the mechanisms affecting recovery, the values determined by Smith *et al.*^[30] were considered in the present study. The test conditions [$\varepsilon = 0.2$ to 0.5, $\dot{\varepsilon} = 0.1$ to 1 s⁻¹, $T_{\text{DEF}} = 1123$ K to 1223 K (850 °C and 950 °C)] and the steel composition (0.16 pct C-1.46 pct Mn-0.4 pct Si-0.03 pct Al) used by these authors were similar to those employed in the present work. They obtained a value of $U_a = 314$ kJ/mol and a value of $K_1 = 0.31$ in Eq. [10]. This value is then used for the determination of V_a from Eqs. [8] and [9]. It should be noted that in Reference 30 a constant value of V_a during softening was assumed, considering the initial internal stress due dislocations, $(\sigma(t) - \sigma_y)$ at $t = 0$, to perform the calculations. The same approach has been taken in the present study.

A commonly used approach for estimating the grain boundary mobility for C-Mn steels is to consider a fraction of Turnbull's pure mobility^[33]:

$$M_{\text{Pure}} = \frac{\delta D_{\text{GB}} V_{\text{M}}}{b^2 RT}, \quad [14]$$

where δ is the grain boundary width (assumed 1 nm), D_{GB} is the grain boundary self-diffusion coefficient [$D_{\text{GB}} = 7.5 \times 10^{-5} \exp\left(\frac{-159000}{RT}\right)$ (m²/s)], R is the gas constant, V_{M} is the molar volume of the austenite [6.85×10^{-6} (m³/mol)], and T is the absolute temperature. This equation, which ignores all possible attachment kinetics, provides an upper estimate for the grain boundary mobility.

In the present work, the value of $M(t)$ in Eq. [4] for the base C-Mn steel was calculated by fitting the $t_{0.5}$ softening time predicted with the model to the experimental value measured at each test temperature. The obtained mobility values are summarized in Table III, together with the ratio to the M_{Pure} given by Eq. [14]. The resulting values are in the range of those considered in other works.^[4,32] However, it must be mentioned that in this case taking an average value of this ratio for the three test temperatures leads to a significant error between the experimental results and the predictions of the model, which indicates that there might be an additional effect of the temperature on this parameter. An increase in this ratio would indicate

an enhanced effect of temperature on reducing mobility as the temperature decreases.

The temperature dependence of the grain boundary mobility calculated for the C2Mn2 steel is shown in Figure 7. As it can be seen, the values can be well fitted to an Arrhenius type relationship of the form $M = M_0 \exp(-Q/RT)$, with $M_0 = 5.03 \text{ m}^4/\text{J} \cdot \text{s}$ and $Q = 264800 \text{ J/mol}$. This type of relationship is usually found to be valid for pure materials, with Q values close to the grain boundary diffusion coefficient. However, in this case, the calculated exponential factor is considerably higher than the grain boundary diffusion coefficient of iron being more closely related to the diffusion activation energies of solute Mn (264 kJ/mol) or to the activation energy for Fe self-diffusion (286 kJ/mol). The supposition implied in the Turnbull estimation, *i.e.*, that during grain boundary migration the atoms transfer in a way that is similar to the elementary action involved in atom transport during grain boundary self diffusion, seems to fail in this case. The relatively high Mn content of this steel (2 pct) could have an effect on retarding mobility as well. As a consequence, the mobility of recrystallizing boundaries would be better explained by solute drag due to manganese atoms.

Therefore, the following equation was used for modeling grain boundary mobility for the base steel:

$$M_{\text{INT}} = 5.03 \exp\left(-\frac{264800}{RT}\right) \quad [15]$$

Figure 8(a) shows the softening evolution predicted by the model (solid lines) compared to measured softening data (symbols). In Figure 7(b), the predictions of the

Table III. Calculated Grain Boundary Mobilities for the C2Mn2 Steel and the Ratio with Respect to the Mobility Calculated by Eq. [14] for a Pure Material

T [K (°C)]	ε	Mobility (m ⁴ /J · s)	$M_{\text{pure}}/\text{Mobility}$
1338 (1065)	0.35	2.26×10^{-10}	1.9
1273 (1000)	0.35	8.86×10^{-11}	2.4
1198 (925)	0.35	1.43×10^{-11}	6.3

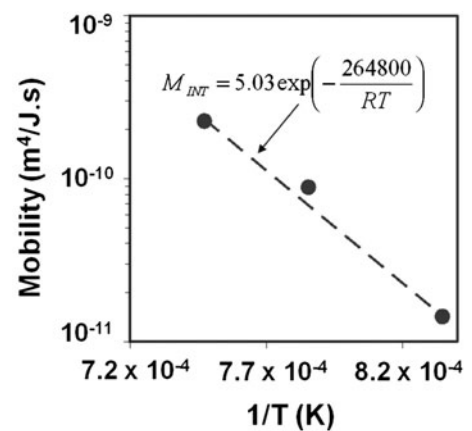


Fig. 7—Temperature dependence of the grain boundary mobility for the C2Mn2 steel.

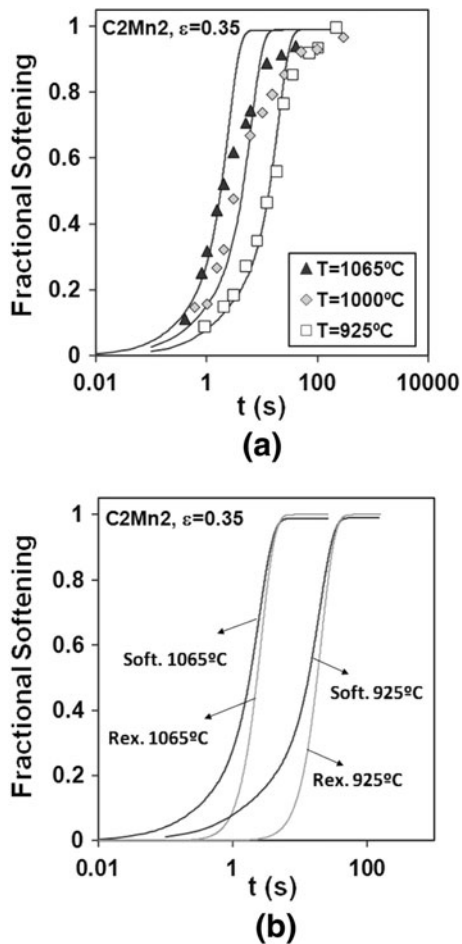


Fig. 8—(a) Comparison between the model predictions and the experimental softening data obtained at different temperatures for the C2Mn2; (b) softening and recrystallization model predictions at 1198 K and 1338 K (925 °C and 1065 °C).

softening and recrystallization models for temperatures of 1338 K and 1198 K (1065 °C and 925 °C) are plotted. From the figure, it can be observed that the softening curves predicted by the model fit reasonably well the experimental results. It can also be noted that the model predicts that the fractional softening levels are of 27 to 30 pct when recrystallization is predicted to start (5 pct), while fractional softening levels of 50 pct correspond to recrystallized fractions of ~27 to 30 pct. These values are in the range of the metallographic measurements above shown for the C2Mn2Al1 steel (see Figure 5).

2. Al-alloyed steels

The above experimental results denote that 1 to 2 pct Al addition leads to noticeable retardation in the softening kinetics in the steels investigated. In order to take into account the retarding effect of solute atoms on the recrystallization kinetics, the model proposed by Cahn^[34] is usually employed. In the model, the steady impurity composition profile of a grain boundary moving at a constant velocity is calculated, and then the composition profile is used to formulate the force exerted by the impurity atoms. By assuming a constant

solute cross-boundary diffusion coefficient and an edge-shaped interaction energy profile, two approximated limiting laws for the drag force can be obtained for high and low boundary velocities (low and high driving forces). In the case of recrystallization after deformation at high temperatures, relatively low driving forces are obtained. In this regime, the model predicts a linear relationship between the driving force and the grain boundary velocity, which allows the following effective mobility for the solute affected grain boundary to be calculated:

$$M_s = \left(\frac{1}{M_{INT}} + \alpha C_s \right)^{-1}, \quad [16]$$

where M_{INT} is the intrinsic mobility of the impurity free material, calculated in this case with Eq. [15], C_s is the impurity concentration and α can be calculated from:

$$\alpha = \frac{\delta N_v (kT)^2}{E_b D} \left(\sinh\left(\frac{E_b}{kT}\right) - \left(\frac{E_b}{kT}\right) \right) \quad [17]$$

δ is the grain boundary width (assumed as 1 nm), N_v is the number of atoms per unit volume [$N_v = 1/V_M = 1.46 \times 10^5$ (m⁻³)], E_b is the binding energy of solute atoms to grain boundaries and D is the cross-boundary diffusion coefficient. According to the model, the main compositional parameters affecting the drag force are the cross-boundary diffusivity, D , and the interaction energy of the solute with the grain boundaries, E_b . The equations shown above indicate that in the low driving force case, impurities with larger absolute E_b values lead to higher drag effects while faster diffusing impurities result in lower drag effect.

The value of E_b can be calculated by assuming that the grain boundary is built up of dislocations from Cottrell's formula^[35,36]:

$$E_b = \frac{4}{3} r_{Fe}^3 \mu \frac{1+v}{1-v} \left| \frac{r_{Fe} - r}{r_{Fe}} \right| \quad [18]$$

where v is the Poisson's ratio for iron and r_{Fe} and r are the atomic radii of iron and of the solute, respectively (Table IV).

Estimating the cross-boundary diffusivity is difficult in general, and it has been approximated as the diffusivity of the solute atoms in the bulk as impurity, D_{Bulk} ,^[4] or as a multiple of this value, with values ranging from $10D_{Bulk}$ ^[37] to $100D_{Bulk}$.^[38] Regarding to Al diffusivity (D_{Bulk}), it must be mentioned that there are significant differences within the diffusion coefficients found in the literature. In the present work, the diffusion coefficient indicated in Table IV^[39] was chosen for the calculations.

The values of D_{Bulk} and E_b determined for Al by applying equation [18] have been plotted against the inverse of the absolute temperature in Figures 9(a) and (b). The values determined for other alloying elements have also been included for comparison in the figure. All the parameters employed in the calculations are listed in Table IV.

Table IV. Bulk Diffusion Coefficients and Atomic Radius of Different Alloying Elements

	Al ^[39]	Mn ^[40]	Nb ^[4]	Si ^[40]	C ^[41]	V ^[40]	
Diffusion coefficient in γ $D_0 \exp\left(\frac{-Q_0}{RT}\right)$							
D_0 (m ² /s)	5.9×10^{-4}	1.78×10^{-5}	8.3×10^{-5}	7×10^{-6}	3.7×10^{-5}	2.8×10^{-5}	
Q_0 (kJ/mol)	241	264	266	243	148	264	
	Fe	Al	Mn	Nb	Si	C	V
Atomic radius (nm) ^[35,42]	0.127	0.1432	0.1312	0.1437	0.1319	0.0916	0.1346

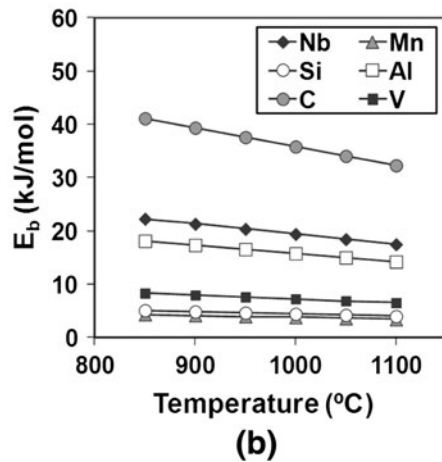
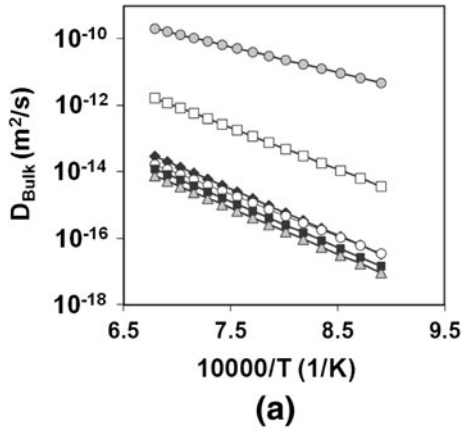


Fig. 9—(a) Bulk impurity diffusion coefficients and (b) calculated binding energies for different alloying and microalloying elements.

The values shown in these graphs agree well with the trends usually reported in the literature for the effect of solutes on the recrystallization kinetics of hot worked austenite. Figure 9(b) shows that Nb, V, Si, and Mn have similar diffusivities, whereas the E_b values are significantly higher for Nb than for the other elements, which is in good agreement with the larger solute retardation potential usually reported for Nb.^[6,43] It can also be noted that the highest binding energy is predicted for C. However, the diffusion coefficient is also the highest. In the case of Al, the E_b values predicted by Eq. [18] range from 16.6 kJ/mol at 1223 K (950 °C) to 14.3 kJ/mol at 1373 K (1100 °C), and they are only slightly lower than those obtained for Nb. However, the reported diffusivity is also significantly

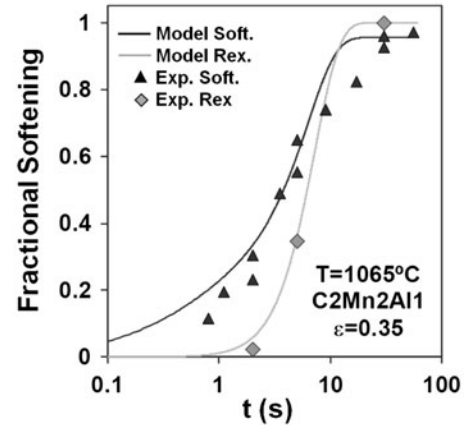


Fig. 10—Comparison between the experimental softening/recrystallization data and the model ($D = 7D_{\text{Bulk}}$) predictions at different temperatures for the C2Mn2Al1 steel.

higher for Al than for Nb or V, Si and Mn. This agrees well with the smaller solute retardation effect assigned to Al relative to Nb for similar additions.^[44] However, it must be remembered that the Al addition levels considered in this work, 1 and 2 pct, are significantly higher than the typical Nb additions found in steels (0.03 to 0.07 pct).

In order to apply the model to the C2Mn2Al1 and C2Mn2Al2 steels, the solute drag retardation effect due to Al addition was estimated through Eqs. [16] and [17] by fitting the calculated 50 pct softening times, $t_{0.5}$, to the experimental data, taking the value of the cross-boundary diffusivity (D) as a fitting factor. An average value of $D = 7D_{\text{Bulk}}$, was obtained. This value is in the range of the values obtained for other microalloying additions.^[37]

In Figure 10, the experimental softening and recrystallized fraction data corresponding to the C2Mn2Al1 steel deformed at 1338 K (1065 °C) and $\epsilon = 0.35$ are compared to the model's predictions. The figure shows fairly good agreement between the experimental and predicted softening data as well as with the metallographic measurements of the recrystallized fraction at these conditions.

Figure 11 shows the comparison between the experimental and predicted softening data for both Al steels at different deformation conditions. Figure 11(a), which corresponds to the C2Mn2Al1 steel deformed with $\epsilon = 0.35$ at different temperatures, shows very good agreement with model. However, in Figure 11(b), which

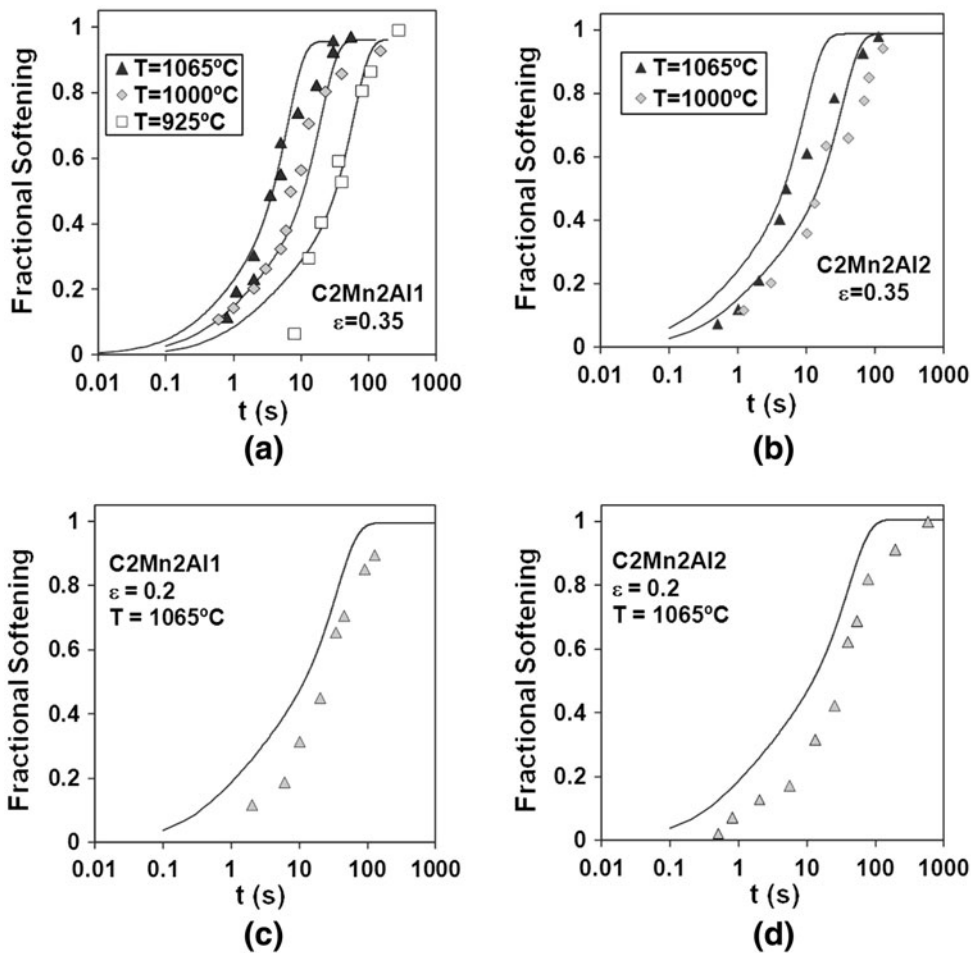


Fig. 11—Comparison between the experimental softening data and the predictions of the model ($D = 7D_{\text{Bulk}}$) at different deformation conditions: (a) and (c) for C2Mn2Al1 steel at $\varepsilon = 0.35$ and $\varepsilon = 0.2$, respectively; (b) and (d) for C2Mn2Al2 at $\varepsilon = 0.35$ and $\varepsilon = 0.2$, respectively.

corresponds to the similarly deformed C2Mn2Al2 steel, although the fit cannot be considered bad, there is a slight tendency for the model to overestimate the softening, mainly at the highest temperature. On the other hand, for both steels and lower deformation $\varepsilon = 0.2$, the model clearly overestimates the experimental softening results (Figures 11(c) and (d)).

Model deviations, which are mainly observed for the highest Al content and lowest strain, suggest a possible overestimation of the calculated recovery kinetics. In the model it is assumed that the recovery rate is only controlled by dislocation glide or climb; however, in the presence of solutes, solute drag could also play a role in recovery. This means that in addition to the retarding effect produced by Al on recrystallization kinetics (modified mobility term), a retardation effect of Al on the recovery rate should also be considered in modeling. Although the effect of solute atoms on recovery has been less studied than their effect on recrystallization, data that indicate that elements like Nb or Mo in solid solution may retard the recovery kinetics of austenite have also been reported.^[7,27] Taking this into account, the effective activation length for the calculation of the activation volume in Eq. [9] should include contributions from both the solute atoms and dislocations. A

simple model, which considers the two contributions added in parallel, is considered here, leading to an equation of the form^[32]:

$$\frac{1}{l_a} = \frac{1}{l_{\text{Disloc}}} + \frac{1}{l_{\text{SD}}} = \frac{\sqrt{\rho}}{K_1} + \frac{C_s^n}{K_2}, \quad [19]$$

where C_s represents the atomic concentration of the solute. The constant K_2 was adjusted by taking the values of $K_1 = 0.31$ and $U_a = 314$ kJ/mol,^[30] as previously used for the C-Mn steel, and $n = 2/3$.^[27] The best fit was achieved with a value of $K_2 = 1 \times 10^{-8}$ and $D = 5D_{\text{Bulk}}$. The results obtained with the modified model at different conditions are shown in Figures 12 and 13. It can be observed that in most cases the predictions improve when using the second approach.

Finally, it can be noted that although the model predictions are significantly improved using this approach, the fit tends to be worse at the highest softening levels both for the C-Mn (Figure 8) and for the Al steels (Figures 12 and 13). In several cases, at long interpass times, the mechanical softening tends to deviate from the predicted curve and the model overestimates the experimental softening. This type of behavior, in which the softening shows retardation at high

softening levels, has also been observed in other cases^[45] and has been attributed to the heterogeneity of the stored energy of deformation. This suggest that the fit

might be improved by assuming a non-uniform stored energy distribution, however, within the simplicity of the model a good fit is obtained for the data considered. It should be taken into account that in the present study, all analyzed microstructures correspond to quenched specimens where the austenitic phase transforms into martensite; therefore, a direct analysis of the strain distribution in the austenite phase cannot be easily performed.

VI. CONCLUSIONS

1. The effect of Al addition on the static softening behavior of C-Mn steels has been characterized. It has been found that Al leads to retardation of the static recrystallization kinetics in C-Mn steels.
2. It has been observed that for the highest Al level and the lowest deformation temperatures, 1238 K and 1198 K (965 °C and 925 °C), austenite to ferrite phase transformation occurred concurrently with mechanical softening, leading to significant retardation of the softening kinetics.

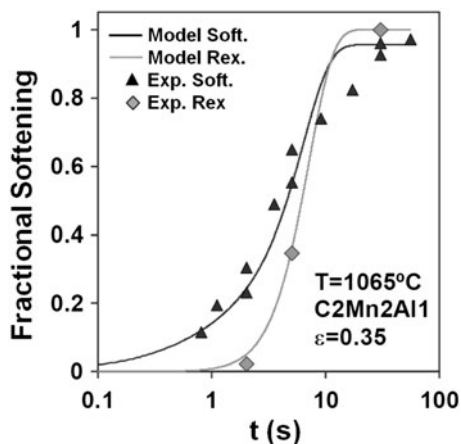


Fig. 12—Comparison between the experimental softening/recrystallization data and the modified model ($D = 5D_{\text{Bulk}}$, $K_2 = 1 \times 10^{-8}$) predictions at different temperatures for the C2Mn2Al1 steel.

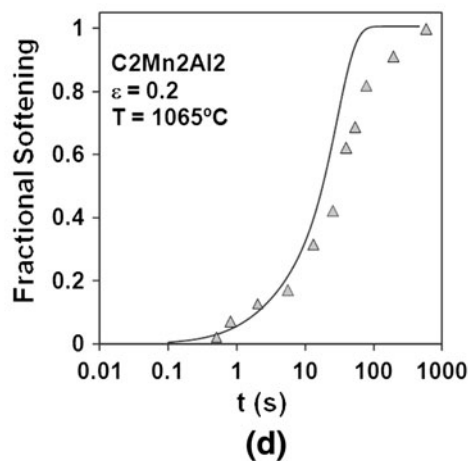
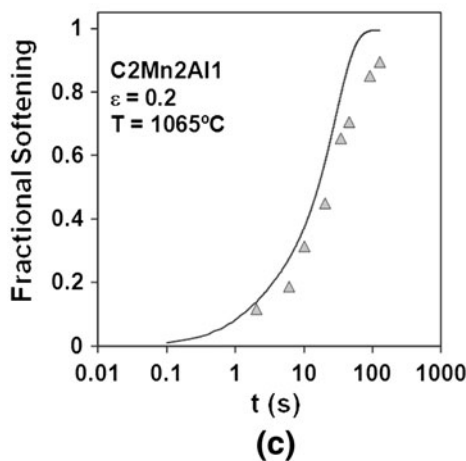
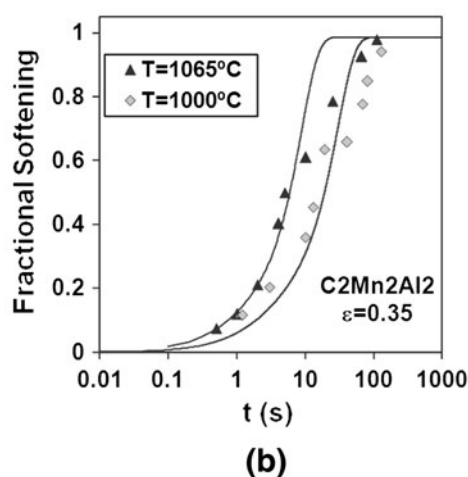
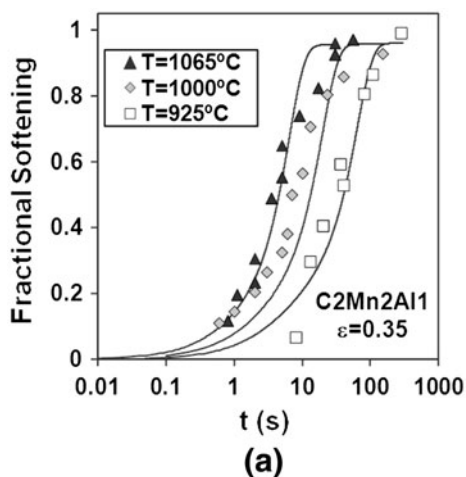


Fig. 13—Comparison between the experimental softening data and the predictions of the modified model ($D = 5D_{\text{Bulk}}$, $K_2 = 1 \times 10^{-8}$) at different deformation conditions: (a) and (c) for C2Mn2Al1 steel at $\epsilon = 0.35$ and $\epsilon = 0.2$, respectively; (b) and (d) for C2Mn2Al2 at $\epsilon = 0.35$ and $\epsilon = 0.2$, respectively.

- The softening kinetics were analyzed using a physically based model from the literature that couples the effect of recovery and recrystallization mechanisms on austenite softening. The main parameters of the model were identified for the present alloys.
- For the base C-Mn steel, the activation volume for recovery, V_a , was considered to be inversely proportional to the initial internal stress due to dislocations. The addition of Al not only produces retardation in recrystallization, but also reduces the recovery rate. In order to capture this effect, the contributions from both the solute atoms and dislocations were considered for the calculation of the activation volume for recovery in the model. V_a was assumed to be inversely proportional to the solute concentration of Al, which resulted in reasonable agreement between the model and the experiment for a variety of deformation conditions.

ACKNOWLEDGMENTS

The authors acknowledge financial support from the European Union, Research Programme of the Research Fund for Coal and Steel (RFSR-CT-2009-00011).

NOMENCLATURE

b	magnitude of the Burgers vector
C_s	solute concentration
D	cross-boundary diffusion coefficient
D_0	initial austenite grain size
D_{Bulk}	bulk diffusion coefficient of the solute in austenite
D_{GB}	grain boundary self-diffusion coefficient
D_{REX}	recrystallized austenite grain size
E	Young's modulus
E_b	binding energy of solute atoms to grain boundaries
F_{REX}	driving force for recrystallization
k	Boltzmann's constant
K_1	constant in Eqs. [9] and [10]
K_2	constant in Eq. [19]
l_a	activation length for the recovery process
l_{Disloc}	activation length for the recovery process due to dislocations
l_{SD}	activation length for the recovery process due to solutes
M	Taylor factor
M_{INT}	grain boundary mobility for the base steel
M_{Pure}	Turnbull's estimate for the mobility of a pure material
M_s	grain boundary mobility for the solute containing material
$M(t)$	grain boundary mobility
n	Avrami exponent
N_{REX}	number of recrystallization nuclei
N_V	number of atoms per unit volume
r	atomic radius of the solute
r_{Fe}	atomic radius of iron
R	gas constant

T	temperature
$t_{0.5}$	time for 50 pct softening fraction
U_a	activation energy of the recovery process
V_a	activation volume of the recovery process
ν	Poisson's ratio for iron
ν_d	Debye frequency
V_M	molar volume of the austenite
X_{REX}	recrystallized fraction
X_{SOFT}	fractional softening
α	interaction parameter in Cahn's solute drag model
α_T	constant of the order of 0.15 (Eq. [6])
δ	grain boundary width
ε	strain
$\dot{\varepsilon}$	strain rate
μ	austenite shear modulus
$\rho(t)$	instantaneous dislocation density
σ_0	flow stress of the completely softened material
σ_m	flow stress of the work hardened material
σ_r	flow stress of the partially softened material
σ_{REX}	yield stress of the fully recrystallized matrix
σ_y	yield stress
$\sigma(t)$	flow stress of the unrecrystallized material
$\tau_{0.5}$	normalized 50 pct softening time

REFERENCES

- C.M. Sellars: *Mater. Sci. Technol.*, 1990, vol. 6, pp. 1072–81.
- A.I. Fernandez, P. Uranga, B. Lopez, and J.M. Rodriguez-Ibabe: *ISIJ Int.*, 2000, vol. 40, pp. 893–901.
- P.D. Hogson and R.K. Gibbs: *ISIJ Int.*, 1992, vol. 32, pp. 1329–38.
- H.S. Zurob, C.R. Hutchinson, Y. Brechet, and G. Purdy: *Acta Mater.*, 2002, vol. 50, pp. 3075–92.
- M.G. Akben, B. Bacroix, and J.J. Jonas: *Acta Metall.*, 1983, vol. 31, pp. 161–74.
- H.L. Andrade, M.G. Akben, and J.J. Jonas: *Metall. Trans. A*, 1983, vol. 14A, pp. 1967–77.
- N. Maruyama, R. Uemori, and M. Sugiyama: *Mater. Sci. Eng. A*, 1998, vol. 250, pp. 2–7.
- M. Gomez, C.I. Garcia, D.M. Haezebrouck, and A.J. DeArdo: *ISIJ Int.*, 2009, vol. 49, pp. 302–11.
- M. De Meyer, D. Vanderschueren, and B.C. De Cooman: *ISIJ Int.*, 1999, vol. 39, pp. 813–22.
- P.J. Jacques, E. Girault, A. Mertens, B. Verlinden, J. van Huumbecq, and F. Delannay: *ISIJ Int.*, 2001, vol. 41, pp. 1061–67.
- A.K. Srivastava, D. Bhattacharjee, G. Jha, N. Gope, and S.B. Singh: *Mater. Sci. Eng. A*, 2007, vols. 445–446, pp. 549–57.
- E.I. Poliak and F. Siciliano: *MS&T 2004 Conference Proceedings*, New Orleans, 2004, pp. 39–45.
- P.P. Suikkanen, V.T.E. Lang, M.C. Somani, D.A. Porter, and L.P. Karjalainen: *ISIJ Int.*, 2012, vol. 52, pp. 471–76.
- A.I. Fernandez, B. Lopez, and J.M. Rodriguez-Ibabe: *Scripta Mater.*, 1999, vol. 40, pp. 543–49.
- Thermodynamic Database TCFE6 – TCS Steels/Fe-Alloys Database, Thermo-Calc.
- G. Glover and C.M. Sellars: *Metall. Trans.*, 1972, vol. 3, pp. 2271–80.
- E.J. Giordani, A.M. Jorge, and O. Balancin: *Scripta Mater.*, 2006, vol. 55, pp. 743–46.
- K.B. Kang, O. Kwon, W.B. Lee, and C.G. Park: *Scripta Mater.*, 1997, vol. 36, pp. 1303–08.
- J.H. Beynon and C.M. Sellars: *ISIJ Int.*, 1992, vol. 32, pp. 359–67.
- R. Abad, A.I. Fernandez, B. Lopez, and J.M. Rodriguez-Ibabe: *ISIJ Int.*, 2001, vol. 41, pp. 1373–82.
- Z. Aretxabaleta, B. Pereda, S.V. Parker, and B. Lopez: in *Proceedings of 4th International Conference on Thermomechanical Processing of Steels*, Sheffield, 2012.

22. F.J. Humphreys and M. Hatherly: *Recrystallization and Related Annealing Phenomena*, 1st ed., Pergamon Press, Oxford, 1995, pp. 188–95.
23. G. Saada: *Acta Metall.*, 1960, vol. 8, pp. 841–47.
24. H.J. Frost and M.F. Ashby: *Deformation Mechanism Maps*, Pergamon Press, Oxford, 1982, pp. 60–70.
25. M. Verdier, Y. Brechet, and P. Guyot: *Acta Mater.*, 1999, vol. 47, pp. 127–34.
26. E. Nes: *Prog. Mater. Sci.*, 1998, vol. 41, pp. 129–93.
27. E. Nes: *Acta Metall. Mater.*, 1995, vol. 43, pp. 2189–207.
28. A. Yoshie, T. Fujita, M. Fujioka, K. Okamoto, and H. Morikawa: *ISIJ Int.*, 1996, vol. 36, pp. 467–73.
29. S. Sarkar and M. Militzer: *Mater. Sci. Technol.*, 2009, vol. 25, pp. 1134–46.
30. A. Smith, A. Miroux, J. Sietsma, and S. Van Der Zwaag: *Steel Res.*, 2006, vol. 77, pp. 595–602.
31. G. Arieta and C.M. Sellars: *Scripta Metall. Mater.*, 1994, vol. 30, pp. 707–12.
32. H. Zurob: Ph.D. Thesis, McMaster University, Canada, 2003.
33. D. Turnbull: *Trans. Am. Inst. Min. Eng.*, 1951, vol. 191, pp. 661–65.
34. J.W. Cahn: *Acta Metall.*, 1962, vol. 10, pp. 789–98.
35. E.A. Simielli, S. Yue, and J.J. Jonas: *Metall. Trans. A*, 1992, vol. 23A, pp. 597–608.
36. A.H. Cottrell: *Dislocations and Plastic Flow in Crystals*, Oxford University Press, Oxford, 1953, p. 57.
37. H.S. Zurob, C.R. Hutchinson, Y. Brechet, and G.R. Purdy: *Mater. Sci. Eng. A*, 2004, vol. 382A, pp. 64–81.
38. C. Iparragirre, A.I. Fernandez, J.M. Rodriguez-Ibabe, and B. Lopez: *Mater. Sci. Forum*, 2007, vols. 539–543, pp. 4119–24.
39. M. Gomez, L. Rancel, and S.F. Medina: *Mater. Sci. Eng. A*, 2009, vol. 506A, pp. 165–73.
40. V. Burachinsky and J.R. Cahoon: *Metall. Mater. Trans. A*, 1997, vol. 28A, pp. 563–82.
41. L. Lissel, G. Engberg, and U. Borggren: in *Proceedings of the 3rd International Conference on Thermomechanical Processing of Steels, 2008*, Associazione Italiana di Metallurgia, Padua, 2001.
42. J.J. Jonas: in *Proceedings of international Conference on Physical Metallurgy of Thermomechanical Processing of Steels and Other Metals*, THERMEC-88, Tokyo, 1988, pp. 59–69.
43. J.J. Jonas: in *High Strength Low Alloy Steels*, D.P. Dunne and T. Chandra, eds., University of Wollongong, Wollongong, 1984, pp. 80–91.
44. H.J. McQueen, S. Yue, N.D. Ryan, and E. Fry: *J. Mater. Process. Technol.*, 1995, vol. 53, pp. 293–310.
45. M. Oyarzabal, A. Martinez de Guerenú, and I. Gutierrez: *Mater. Sci. Eng. A*, 2008, vol. 485A, pp. 200–09.